PCCP

Accepted Manuscript




ROYAL SOCIETY OF CHEMISTRY

www.rsc.org/pccp

PCCP

RSCPublishing

COMMUNICATION

# Photoelectrochemical Reduction of Aqueous Protons With a CuO|$CuBi_2O_4$ Heterojunction Under Visible Light Irradiation

Cite this: DOI: 10.1039/x0xx00000x

Received 00th January 2014,
Accepted 00th January 2014

DOI: 10.1039/x0xx00000x

www.rsc.org/

Hyun S. Park,[a] Chong-Yong Lee,[a] and Erwin Reisner*[,a]

**A p-type heterojunction photoelectrode consisting of platinized $CuBi_2O_4$ layered on a CuO film was prepared. The CuO|$CuBi_2O_4$|Pt electrode photo-generates $H_2$ in pH neutral aqueous solution during visible light irradiation and exhibits a substantially enhanced photocurrent compared to CuO|Pt and $CuBi_2O_4$|Pt electrodes. Reduced electron-hole recombination by the band offsets in the heterostructure is responsible for the improved photoelectrochemical performance of CuO|$CuBi_2O_4$ with a small band-gap of approximately 1.5 eV.**

The development of an efficient, stable, and scalable photocatalyst for the conversion of solar energy into chemical energy is a major goal to address the energy challenge of this century. Photolysis of water into $H_2$ and $O_2$ on semiconductors has been studied for decades,[1] and current efforts focus on the discovery of small band-gap photocatalysts with high activity during visible light irradiation.

Theoretically, a band-gap of less than 1.8 eV would allow for a photon-to-$H_2$ conversion efficiency of more than 20%.[2, 3] A common strategy to achieve high efficiency is pairing a small band-gap photocathode for $H_2$ production with a semiconductor photoanode with complementary light absorption for water oxidation.[4, 5] Beyond efficiency, the semiconductor electrodes must also be made of inexpensive materials, easy to fabricate and display long-term stability in aqueous electrolyte solution.[6]

Despite a large number of encouraging n-type photoanodes being available,[7-11] there are only a few promising candidates for efficient p-type photocathodes for the $H_2$ evolution reaction (HER). Many p-type semiconductors, e.g., p-doped Si,[12] $Cu_2O$,[13-15] InP,[16] $Cu_2ZnSnS_4$,[17] $CuIn_xGa_{1-x}Se_2$,[18] $WSe_2$,[19] $CuRhO_2$,[20] CuO,[21] and $CuBi_2O_4$,[22-24] have been discussed for the photoelectrochemical (PEC) HER using solar energy. However, these photocathodes have currently restricted utility due to their high cost and/or rapid photo-decomposition in aqueous solution.

$CuBi_2O_4$ is a natural mineral semiconductor with a tetragonal structure, which is (photo-)chemically unstable in acidic and pH neutral aqueous solution.[23, 25] Despite the attractive band-gap size of approximately 1.5 to 1.8 eV of the p-type semiconductor, there is only a limited number of studies where $CuBi_2O_4$ was employed as a photoelectrocatalyst.[22-24] CuO is another attractive and promising p-type semiconductor with a small band-gap.[26, 27] It has a conduction band position suitable for HER and has been used as coating on $TiO_2$ and $Cu_2O$ for visible light absorption and to improve the photochemical stability of the electrode, respectively.[28, 29] However, CuO and $CuBi_2O_4$ suffer from severe photodegradation in aqueous solution through photoreduction to metallic copper.[23]

Herein, we report on the facile preparation of an inexpensive photocathode based on a CuO|$CuBi_2O_4$ heterojunction coated with Pt for visible light promoted HER in pH neutral aqueous electrolyte solution (Figure 1). The enhanced photocurrent is the result of improved electron-hole separation by utilizing the valence band offsets at the heterojunction interface and the Pt-layer enhanced the photostability of the CuO|$CuBi_2O_4$ heterojunction.

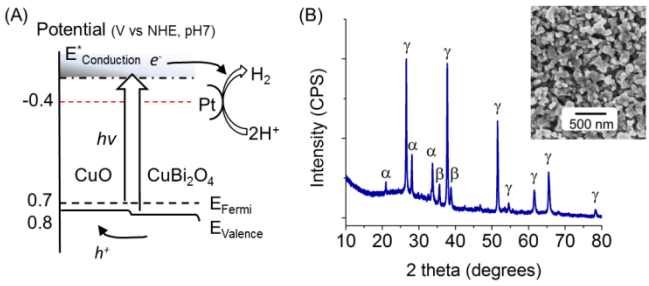


Figure 1. (A) Schematic energy diagram of the estimated band-edge positions of CuO|$CuBi_2O_4$|Pt heterojunction. (B) Powder X-ray diffraction patterns of CuO|$CuBi_2O_4$ heterojunction (α=$CuBi_2O_4$, PDF#48-1886; β=CuO, PDF#44-0706; and γ=FTO). Inset in (B) shows an SEM image of CuO|$CuBi_2O_4$ electrode surface.

CuO, $CuBi_2O_4$ and CuO|$CuBi_2O_4$ thin film electrodes were prepared by drop-casting the precursor solution ($Cu(NO_3)_2$ and $Bi(NO_3)_3$ in ethylene glycol) onto fluorine-doped tin oxide (FTO)-coated glass followed by heat treatment at 500 °C in air (see Electronic Supporting Information for experimental details and characterization). X-ray diffraction patterns show monoclinic CuO (PDF#44-0706) and Kusachiite tetragonal $CuBi_2O_4$ (PDF#48-1886) without secondary phase formation in the homo-layered and heterostructured thin film electrodes (Figure 1 and S1). The crystal size observed by scanning electron microscopy (SEM) was

approximately 100 nm for the FTO|CuO and FTO|CuO|$CuBi_2O_4$ heterojunction films, whereas a smooth surface was observed for the FTO|$CuBi_2O_4$ film (Figure 1 and S2). The FTO|CuO|$CuBi_2O_4$ heterojunction film shows a porous structure similar to that of FTO|CuO with a film thickness of about 300 nm as shown in the cross section image in Figure S2.

The photoactivity of the Pt-free electrodes was first studied by linear sweep voltammetry (LSV) and chronoamperometry (CA) at 0.2 V vs. normal hydrogen electrode (NHE) in a pH 6.8 aqueous solution (Figures S3 and S4). An AM 1.5G solar light irradiator with a UV-vis light intensity of 100 mW $cm^{-2}$ was employed. As expected, FTO|CuO, FTO|$CuBi_2O_4$, and FTO|CuO|$CuBi_2O_4$ showed poor photo-stability due to the photodecomposition of electrodes during irradiation. (Figure S4). The photocurrent onset at FTO|$CuBi_2O_4$ in LSV runs was observed at approximately 100 mV more positive potential compared to FTO|CuO (Figure S3). The positive onset potential of the FTO|$CuBi_2O_4$ electrode indicates a more positive flat-band or valence band edge potential of FTO|$CuBi_2O_4$, in agreement with previous reports in the literature.[23, 24] Mott-Schottky plot analysis resulted in a flat-band potential of CuO and $CuBi_2O_4$ of 0.69±0.01 V and 0.81±0.03 V *vs.* NHE in neutral aqueous electrolyte solution (Figure S5), respectively, which is in agreement with the onset potentials in the LSV measurements.

PEC experiments with the FTO|CuO, FTO|$CuBi_2O_4$ and FTO|CuO|$CuBi_2O_4$ heterojunction electrodes in acetonitrile solution in the presence of an electron acceptor, ethyl viologen diperchlorate ($EV^{2+}$), were subsequently performed to avoid photodegradation in water with the bare metal oxide electrodes (Figures S6 and S7).[6,24,30] The photocurrent measured under these conditions did not contain any background current from electrode photodecomposition and was therefore smaller than in the aqueous solution. Consequently, the FTO|CuO and FTO|$CuBi_2O_4$ electrodes show stable photocurrent without noticeable photodegradation in acetonitrile solution (Figure S7). The steady-state photocurrent measured by CA was only approximately 30% of the transient photocurrent for all electrodes measured by LSV and the large transient behavior, including peak-shaped photocurrent response in the LSV, indicates significant surface recombination at the photocathodes and visible light absorption by $EV^{+}$ formed at the electrode surface.[31] Investigation of systematic surface passivation would be an efficient method to further reduce the recombination rate at surface defects and leading to an enhanced photocurrent.

The effect of different amounts of the Cu-based semiconductors deposited on FTO on the photocurrent was also studied in acetonitrile with $EV^{2+}$ for each electrode (Figure S7). The optimized amount of metal ions was 2.2, 0.45, and 2.2|0.45 µmol $cm^{-2}$ for CuO, $CuBi_2O_4$, and CuO|$CuBi_2O_4$, respectively, used for electrode preparations in further experiments (cross-section images and film thickness are shown in Figure S2). Thicker films resulted in a decreased photocurrent response or physical instability.

The CuO|$CuBi_2O_4$ heterojunction displayed a substantially higher photocurrent in LSV and CA measurements than the homo-layered FTO|CuO or FTO|$CuBi_2O_4$ electrodes (Figure 2, S6, S7, and S8). For example, a three times higher photocurrent was obtained with the CuO|$CuBi_2O_4$ heterojunction for $EV^{2+}$ reduction than with the homo-layered electrodes at –0.45 V *vs*. NHE (Figure S7).

The higher photocurrent results from better electron-hole separation in the CuO|$CuBi_2O_4$ heterojunction than in CuO or $CuBi_2O_4$ for the following reasons: the photocurrent at FTO|CuO or FTO|$CuBi_2O_4$ was not limited by light absorption (thickness dependence in Figure S7D) and not hindered by the reaction kinetics for $EV^{2+}$ reduction.[30] The gradual increase of photocurrent observed at the CuO|$CuBi_2O_4$ heterojunction during CA can be assigned to a structural changes at the CuO and $CuBi_2O_4$ interface (Figure S7C and S9).[32]

The Pt electrocatalyst was then photo-deposited on the electrodes from an aqueous $K_2PtCl_4$ solution (see ESI and Figure S10) in order to enhance the activity and stability of the photocathodes in aqueous electrolyte solution during illumination.[33-35]

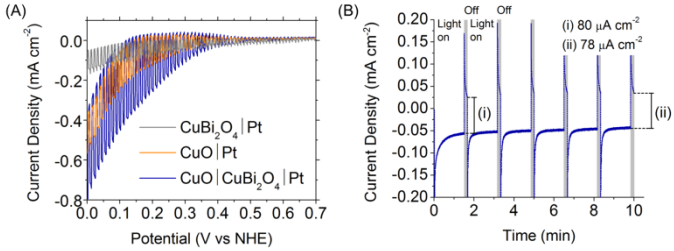


Figure 2. (A) Photocurrent response of FTO|CuO|Pt, FTO|$CuBi_2O_4$|Pt and FTO|CuO|$CuBi_2O_4$|Pt electrodes at a scan rate of 20 mV $s^{-1}$ under chopped visible light irradiation (λ > 420 nm) and (B) CA runs of FTO|CuO|$CuBi_2O_4$|Pt electrode under visible light irradiation for 10 min (pH 6.8, 0.3 M $K_2SO_4$, 0.1 M phosphate, deaerated). CA was measured with an applied potential of 0.2 V vs. NHE to the photocathodes.

LSV scans for FTO|$CuBi_2O_4$|Pt, FTO|CuO|Pt and FTO|CuO|$CuBi_2O_4$|Pt measured in pH 6.8 aqueous solution are shown in Figures S8 (UV-vis irradiation) and 2 (λ > 420 nm). Photocurrents at FTO|CuO|$CuBi_2O_4$|Pt were more than twice as high as at FTO|CuO|Pt and FTO|$CuBi_2O_4$|Pt. In addition, the Pt-modified electrodes exhibited a small improvement in photostability compared to the Pt-free electrodes and reduced photodegradation was observed after 10 min irradiation in the aqueous solution (Figure 2 and S11). A steady-state photocurrent of 100 and 80 µA $cm^{-2}$ was observed during CA for the FTO|CuO|$CuBi_2O_4$|Pt electrode under UV-vis and visible light (λ > 420 nm) irradiation, respectively. Thus, approximately 80% of the photocurrent is generated by λ > 420 nm light absorption at the heterojunction electrode (Figure 3). However, photocurrents with FTO|CuO|$CuBi_2O_4$|Pt do still not display long term stability and currents started to decrease quickly after approximately 10 min, with approximately 60% of the photocurrent remaining after 20 min (Figure S11D). The photo-instability of FTO|CuO|$CuBi_2O_4$|Pt originates presumably from non-conformal coating of the electrocatalyst on the photocathode and the resulting lack of complete protection from the electrolyte solution (Figure S10).[19, 36, 37] LSV scans also indicate a non-negligible dark current with FTO|CuO|$CuBi_2O_4$|Pt and FTO|CuO|Pt electrodes (Figure 2A), which indicates possible reduction of the photocathodes. Studies to ensure longer time stability of photocathodes with conformal and noble-metal free coatings in aqueous solution are currently in progress in our laboratory.

Mott-Schottky plots of FTO|CuO and FTO|$CuBi_2O_4$ allowed us to determine the flat-band potentials of the heterojunction, which is closely placed to the valence band edge for a heavily p-doped semiconductor such as CuO and $CuBi_2O_4$. The size of the band gap, or position of conduction band-edge of CuO and $CuBi_2O_4$ could not be unambiguously determined by UV-vis absorption spectroscopy and Tauc plots (Figure S12) and is not precisely known from the literature.[22-24, 38] CuO was reported with a wide range of indirect band gap of 1.2 to 1.9 eV[24, 38] and $CuBi_2O_4$ with a band gap between 1.5 to 1.8 eV.[23, 39] We expect the band-gap size to be larger than 1.2 eV for CuO and greater than 1.3 eV for $CuBi_2O_4$ based on the observed photoreduction of $EV^{2+}$ and proton reduction reactions both at the FTO|CuO and FTO|$CuBi_2O_4$ electrodes as shown in Figure 2 and S6.

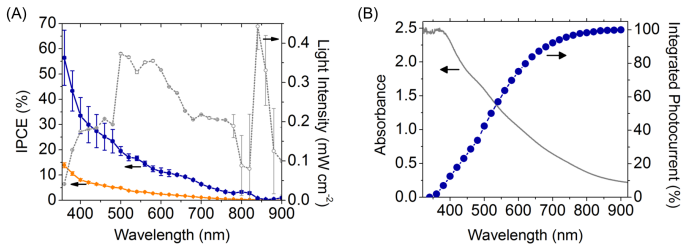


Figure 3. (A) IPCE plots at 0 (blue) and 0.2 V vs. NHE (orange) and light intensity (grey) at different wavelengths. (B) UV-vis absorption spectrum (solid line) and integrated photocurrent over the wavelength based on IPCE from (A) at 0 V (blue circles) of $CuO|CuBi_2O_4|Pt$ in a deaerated aqueous solution (0.3 M $K_2SO_4$, pH 6.8, 0.1 M phosphate).

The valence band offsets or internal electric field given in the heterojunction indicates that enhanced electron-hole separation can occur in the heterostructured electrode of CuO and $CuBi_2O_4$. The heterojunction of $FTO|CuO|CuBi_2O_4|Pt$ generates at least twice the photocurrent of homo-layered FTO|CuO|Pt or $FTO|CuBi_2O_4|Pt$ electrodes due to the reduction of electron-hole recombination by the band offsets provided in the heterostructure. In contrast, a deteriorating effect was observed with an inverted heterojunction, i.e., $FTO|CuBi_2O_4|CuO$. With this electrode, a reduced photocurrent results from the deep valence band of $CuBi_2O_4$ and the resulting trapping of holes and increased electron-hole recombination at the interfaces between the $CuBi_2O_4$ and CuO layers (Figure S13).

$H_2$ generation at the photocathodes was confirmed by electrochemical detection of $H_2$ (Figure S14): a Pt ultramicroelectrode (UME) with a diameter of 100 µm with an applied potential of –0.3 V for $H_2$ oxidation was placed near (at an estimated distance of approximately 500 µm) the $FTO|CuO|CuBi_2O_4|Pt$ electrode to detect $H_2$ during back-side irradiation of the photocathode (see Experimental Section in ESI for details). Thereby, $H_2$ diffuses from the photoelectrode to the Pt UME and the $H_2$ oxidation current at the latter is proportional to the $H_2$ evolved at the former electrode. Note that the $FTO|CuO|CuBi_2O_4|Pt$ electrode has a small electrode area and was largely covered by an insulating epoxy resin resulting in a small current in Figure S14. A $H_2$ oxidation current was observed at the Pt UME upon irradiation of the $FTO|CuO|CuBi_2O_4|Pt$ electrode. The electrooxidation current at Pt demonstrates $H_2$ evolution at the photocathode.

The electrocatalyst Pt on the heterojunction facilitates the reaction kinetics for HER and fewer photoexcited electrons are consumed for the electrode decomposition reactions shown in Eqs. 1 and 2.[13] We note that $H_2$ was only detected at the Pt UME with the $FTO|CuO|CuBi_2O_4|Pt$ photocathode, but not at $FTO|CuO|CuBi_2O_4$ without Pt, where the photocurrents are mainly due to photodecomposition of the heterojunction electrode.[11,13,19, 36,40] Previously, photoelectrodeposition of electrocatalyst layers, *e.g.* Ru and Pt onto p-$WSe_2$ for HER[19] or Co-Pi on Ba-doped $Ta_3N_5$ for OER[33], were used to fabricate the protective layers to reduce the photodecomposition reactions and to utilize electrons and holes primarily for HER and OER.

$$2CuO + H_2O + 2e^- \rightarrow 2Cu_2O + 2OH^- \ (E^0 = 0.20V \text{ vs. NHE}) \quad (1)$$
$$Cu_2O + H_2O + 2e^- \rightarrow 2Cu + 2OH^- \quad (E^0 = 0.07V \text{ vs. NHE}) \quad (2)$$

Incident photon to current conversion efficiencies (IPCE) of $FTO|CuO|CuBi_2O_4|Pt$ with UV-vis absorption spectra shown in Figure 3 indicate an excellent visible light response of the heterojunction electrode (see ESI for details). The heterojunction electrode shows maximum IPCE of 60% at 0 V for high-energy photon absorption, and shows a visible response at the wavelength up to 850 nm. The effective band-gap size of $FTO|CuO|CuBi_2O_4|Pt$ electrode is therefore approximately 1.5 eV based on IPCE measurements. In addition, integration of the photocurrent over the wavelength from the IPCE measurements in Figure 3A further confirmed the efficient visible light harvesting of the heterojunction electrode (Figure 3B). Figure 3B shows the wavelength dependent photocurrent produced by absorbed photons. More than 80% of the photocurrent was generated by visible light irradiation with wavelength longer than 420 nm. The visible light response of the heterojunction in LSVs is also shown in Figure S15. IPCE values at various applied potentials in Figure S16 show that the photoactivity enhancement in the heterojunction electrode appeared under monochromatic irradiation agrees well with the visible light response in Figure 2. Note that the beam intensities used for IPCE measurements indicated in Figure 3A were different from the AM 1.5 irradiance, which can affect IPCE values.[41]

In summary, a $CuO|CuBi_2O_4|Pt$ electrode for visible light driven $H_2$ evolution in aqueous electrolyte solution is reported. The novel heterojunction electrode structure reduces charge recombination, has a narrow band-gap of approximately 1.5 eV and can be stabilized in water with a suitable electrocatalyst layer. $CuO|CuBi_2O_4$ is also easy to assemble, does not contain prohibitively expensive materials and is therefore a promising candidate for visible absorption and charge-separation in solar-to-fuel conversion devices with theoretical efficiencies of more than 20%.[2, 3] CuO and $CuBi_2O_4$ form an excellent heterojunction pair, which more than doubles the photoactivity compared to the corresponding monolayer electrodes. Work to further increase the performance and stability of photoelectrodes in aqueous solution and replacement of Pt by inexpensive electrocatalysts is currently in progress in our laboratory.

## Notes and references

[a] *Christian Doppler Laboratory for Sustainable SynGas Chemistry, Department of Chemistry, University of Cambridge, Lensfield Road, Cambridge CB2 1EW, United Kingdom. E-mail: reisner@ch.cam.ac.uk*

† Electronic Supplementary Information (ESI) available: Experimental details and additional results including photoelectrochemical measurements and material characterizations of electrodes. See DOI: 10.1039/c000000x/

## Acknowledgments

The work at Cambridge was supported by the Christian Doppler Research Association (Austrian Federal Ministry of Economy, Family and Youth and National Foundation for Research, Technology and Development), the OMV Group the EPSRC (EP/H00338X/2) and BBSRC (BB/K010220/1).

1. A. Fujishima and K. Honda, *Nature*, 1972, **238**, 37-38.
2. M. C. Hanna and A. J. Nozik, *J. Appl. Phys.*, 2006, **100**, 074510.
3. M. F. Weber and M. J. Dignam, *Int. J. Hydrogen. Energ.*, 1986, **11**, 225-232.
4. J. Brillet, J.-H. Yum, M. Cornuz, T. Hisatomi, R. Solarska, J. Augustynski, M. Graetzel and K. Sivula, *Nat. Photon.*, 2012, **6**, 824-828.
5. O. Khaselev and J. A. Turner, *Science*, 1998, **280**, 425-427.
6. A. J. Bard and M. S. Wrighton, *J. Electrochem. Soc.*, 1977, **124**, 1706-1710.

7. C. Yang, Z. Wang, T. Lin, H. Yin, X. Lu, D. Wan, T. Xu, C. Zheng, J. Lin, F. Huang, X. Xie and M. Jiang, *J. Am. Chem. Soc.*, 2013, **135**, 17831-17838.
8. K. Sivula, R. Zboril, F. Le Formal, R. Robert, A. Weidenkaff, J. Tucek, J. Frydrych and M. Grätzel, *J. Am. Chem. Soc.*, 2010, **132**, 7436-7444.
9. H. S. Park, K. C. Leonard and A. J. Bard, *J. Phys. Chem. C*, 2013, **117**, 12093-12102.
10. J. A. Seabold and K.-S. Choi, *Chem. Mater.*, 2011, **23**, 1105-1112.
11. Y.-H. Lai, T. C. King, D. S. Wright and E. Reisner, *Chem. Eur. J.*, 2013, **19**, 12943-12947.
12. E. L. Warren, J. R. McKone, H. A. Atwater, H. B. Gray and N. S. Lewis, *Energy Environ. Sci.*, 2012, **5**, 9653-9661.
13. A. Paracchino, V. Laporte, K. Sivula, M. Gratzel and E. Thimsen, *Nat. Mater.*, 2011, **10**, 456-461.
14. M. Hara, T. Kondo, M. Komoda, S. Ikeda, J. N. Kondo, K. Domen, M. Hara, K. Shinohara and A. Tanaka, *Chem. Commun.*, 1998, 357-358.
15. C.-Y. Lin, Y.-H. Lai, D. Mersch and E. Reisner, *Chem. Sci.*, 2012, **3**, 3482-3487.
16. M. H. Lee, K. Takei, J. Zhang, R. Kapadia, M. Zheng, Y.-Z. Chen, J. Nah, T. S. Matthews, Y.-L. Chueh, J. W. Ager and A. Javey, *Angew. Chem. Int. Ed.*, 2012, **51**, 10760-10764.
17. D. Yokoyama, T. Minegishi, K. Jimbo, T. Hisatomi, G. Ma, M. Katayama, J. Kubota, H. Katagiri and K. Domen, *Appl. Phys. Express*, 2010, **3**, 101202.
18. T. J. Jacobsson, V. Fjallstrom, M. Sahlberg, M. Edoff and T. Edvinsson, *Energy Environ. Sci.*, 2013, **6**, 3676-3683.
19. J. R. McKone, A. P. Pieterick, H. B. Gray and N. S. Lewis, *J. Am. Chem. Soc.*, 2012, **135**, 223-231.
20. J. Gu, Y. Yan, J. W. Krizan, Q. D. Gibson, Z. M. Detweiler, R. J. Cava and A. B. Bocarsly, *J. Am. Chem. Soc.*, 2013, **136**, 830-833.
21. A. Kargar, Y. Jing, S. J. Kim, C. T. Riley, X. Pan and D. Wang, *ACS Nano*, 2013, **7**, 11112-11120.
22. T. Arai, Y. Konishi, Y. Iwasaki, H. Sugihara and K. Sayama, *J. Comb. Chem.*, 2007, **9**, 574-581.
23. N. T. Hahn, V. C. Holmberg, B. A. Korgel and C. B. Mullins, *J. Phys. Chem. C*, 2012, **116**, 6459-6466.
24. S. P. Berglund, H. C. Lee, P. D. Nunez, A. J. Bard and C. B. Mullins, *Phys. Chem. Chem. Phys.*, 2013, **15**, 4554-4565.
25. C. Henmi, *Mineral. Mag.* , 1995, **59**, 545-548.
26. J. Bandara, I. Guasaquillo, P. Bowen, L. Soare, W. F. Jardim and J. Kiwi, *Langmuir*, 2005, **21**, 8554-8559.
27. Z. Zhang and P. Wang, *J. Mater. Chem.*, 2012, **22**, 2456-2464.
28. D. Praveen Kumar, M. V. Shankar, M. Mamatha Kumari, G. Sadanandam, B. Srinivas and V. Durgakumari, *Chem. Commun.*, 2013, **49**, 9443-9445.
29. A. Radi, D. Pradhan, Y. Sohn and K. T. Leung, *ACS Nano*, 2010, **4**, 1553-1560.
30. H. Ye, H. S. Park, V. A. Akhavan, B. W. Goodfellow, M. G. Panthani, B. A. Korgel and A. J. Bard, *J. Phys. Chem. C*, 2011, **115**, 234-240.
31. L. M. Peter, *Chem. Rev.*, 1990, **90**, 753-769.
32. I. Hwang, C. R. McNeill and N. C. Greenham, *J. Appl. Phys.*, 2009, **106**, 094506.
33. Y. Li, L. Zhang, A. Torres-Pardo, J. M. González-Calbet, Y. Ma, P. Oleynikov, O. Terasaki, S. Asahina, M. Shima, D. Cha, L. Zhao, K. Takanabe, J. Kubota and K. Domen, *Nat. Commun.*, 2013, **4**.
34. E. M. P. Steinmiller and K.-S. Choi, *Proc. Natl. Acad. Sci. USA*, 2009, **106**, 20633-20636.
35. B. Kraeutler and A. J. Bard, *J. Am. Chem. Soc.*, 1978, **100**, 4317-4318.
36. C. G. Morales-Guio, S. D. Tilley, H. Vrubel, M. Gratzel and X. Hu, *Nat. Commun.*, 2014, **5**, 3059.
37. B. Seger, A. B. Laursen, P. C. K. Vesborg, T. Pedersen, O. Hansen, S. Dahl and I. Chorkendorff, *Angew. Chem. Int. Ed.*, 2012, **51**, 9128-9131.
38. D. Wu, Q. Zhang and M. Tao, *Phys. Rev. B*, 2006, **73**, 235206.
39. T. Arai, M. Yanagida, Y. Konishi, Y. Iwasaki, H. Sugihara and K. Sayama, *J. Phys. Chem. C*, 2007, **111**, 7574-7577.
40. S. Y. Reece, J. A. Hamel, K. Sung, T. D. Jarvi, A. J. Esswein, J. J. H. Pijpers and D. G. Nocera, *Science*, 2011, **334**, 645-648.
41. Y. Nosaka and M. A. Fox, *J. Phys. Chem.*, 1986, **90**, 6521-6522.

# Table of Contents artwork